https://doi.org/10.15407/ujpe68.11.772

K. VIJAYA KUMAR,[1] S.D. BHAVANI[2]

[1] Department of Physics, JNTUH University College of Engineering Jagtial, Nachupally (Kondagattu)
(Jagtial District – 505501, Telangana, India; e-mail: kvkphd@gmail.com)
[2] Department of Chemistry, Government Degree College Rajendranagar
(Rangareddy District – 501218, Telangana, India)

EFFECT OF CALCINATION TEMPERATURE AND SUBSTITUTION OF ERBIUM ON STRUCTURAL AND OPTICAL PROPERTIES OF NICKEL ZINC FERRITE NANOPARTICLES

A single composition of erbium-doped nickel zinc ferrite $Ni_{0.5}Zn_{0.5}Fe_{1.95}Er_{0.05}O_4$ is synthesized by the sol-gel autocombustion process. The prepared composition was divided into five equal parts. One of the parts was an as-prepared sample, and remaining four other parts were calcinated at 600, 700, 800, and 900 °C to investigate the variation in structural and optical properties with the calcination temperature. The structural characterization was performed using XRD and SEM. Optical properties were analyzed using FTIR and UV-Visible spectral data. XRD patterns confirm the spinel cubic crystal structure and the Fd3m space group. The crystallite size was minimum for the as-prepared sample (17.9452 nm), and the crystallite size was maximum for the sample calcinated at 900 °C (29.8481 nm). SEM images revealed the grain size in the interval from 55.38 nm to 177.73 nm, and certain nanotubes were formed in the sample calcinated at 800 °C. Optical energy band gap was observed in the interval from 5.556 eV to 3.969 eV. All these testifies to the variations in structural and optical properties of $Ni_{0.5}Zn_{0.5}Fe_{1.95}Er_{0.05}O_4$ with the calcination temperature.

K e y w o r d s: ferrite, sol-gel, calcination temperature, structural and optical properties.

1. Introduction

The general chemical formula for spinel ferrite materials is AB_2O_4, where A and B denote different metal cations at tetrahedral (A site) and octahedral (B site) positions, respectively. The types, amounts, and locations of the metal cations in the crystalline structure have a major effect on the physicochemical properties of ferrites [1–2]. Nanocrystalline magnetic materials have drawn interest from a variety of disciplines, including physics, chemistry, biology, medicine, materials science, and engineering because of their exceptional and distinctive qualities. When compared to their bulk counterparts, nanomaterials exhibit the altered or enhanced reactivity and useful thermal, mechanical, optical, electrical, and magnetic properties due to their high surface-to-volume ratio and particle sizes of up to 100 nm [3–6]. These spinal ferrites are one of the successful magnetic nanoparticles (MNPs) for various applications such as magnetic devices, supercapacitors, batteries, refrig-

C i t a t i o n: Vijaya Kumar K., Bhavani S.D. Effect of calcination temperature and substitution of erbium on structural and optical properties of nickel zinc ferrite nanoparticles. *Ukr. J. Phys.* **68**, No. 11, 772 (2023). https://doi.org/10.15407/ujpe68.11.772.

Цитування: Віджая Кумар К., Бхавані С.Д. Вплив температури кальцинування і домішки ербію на структурні та оптичні властивості наночастинок фериту, що містить нікель та цинк. *Укр. фіз. журн.* **68**, №11, 774 (2023).

erators, magnetocaloric refrigerators, photocatalysis [7–12], catalysts [13–14], magnetic resonance imaging (MRI) [15], magnetic fluid hyperthermia [16], and cancer therapy [17–18]. Several researchers have used different techniques to examine the properties and to see the effect of synthesis techniques, as well as a doping element, on the structural, optical, magnetic, and dielectric properties. The substitution of rare earth ions (RE) into the spinel ferrites gives interesting properties compared to other substituted ferrites [19]. Several researchers have reported that the rare earth doping in ferrites causes a structural distortion, thereby significantly changing the properties [20–22]. As it known, the rare earth ions have unpaired 4f electrons. When RE ions occupy the ferrite lattice sites, the RE-Fe interaction, i.e., the 3d–4f coupling, leads to the enhanced magnetic, optical, and electrical properties. In this present work, the erbium-doped nickel zinc ferrite $Ni_{0.5}Zn_{0.5}Fe_{1.95}Er_{0.05}O_4$ was-prepared using the sol-gel method and was- calcinated at various temperatures to investigate the variation in structural and optical properties with calcination temperature.

2. Experimental

The erbium-doped nickel zinc ferrite with the composition $Ni_{0.5}Zn_{0.5}Fe_{1.95}Er_{0.05}O_4$ sample was-prepared by the sol-gel autocombustion [23] following the flow chart, as shown in Fig. 1. zinc nitrate ($Zn(NO_3)_2 \cdot 6H_2O$), iron nitrate ($Fe(NO_3)_3 \cdot 9H_2O$), nickel nitrate $Ni(NO_3)_2 \cdot 6H_2O$), erbium nitrate ($Er(NO_3)_3$), citric acid, and ammonia of the analytical grade were used as starting materials. A stoichiometric solution of nickel nitrate, ferric nitrate, and erbium nitrate were prepared. To chelate Zn^{2+}, Ni^{2+}, Fe^{3+}, and Er^{3+} ions in the solution, citric acid was added.

The molar ratio 1 : 3 was adjusted between the citric acid and the total moles of metal nitrate ions. P^H of the solution was adjusted to 7 by adding the ammonia in the adequate amount. Then the solution was heated on a hot plate with a continuous stirring at about 100 °C until viscous gel is formed. Then the temperature was raised to about 200 °C, which leads to the self-propagating combustion reaction resulted in the formation of a loose powder [24–25]. Then the obtained powder was divided into five equal proportions. Among them, one proportion was treated as the as-prepared sample, and the other four proportions were calcinated at four different temperatures for 8 hours, with temperature range from 600 to 900 °C.

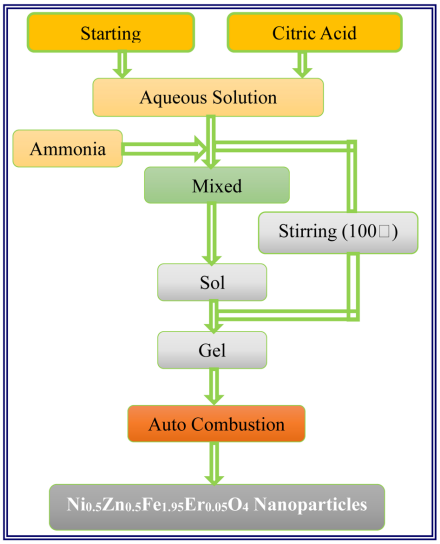

Fig. 1. Flowchart of synthesis of $Ni_{0.5}Zn_{0.5}Fe_{1.95}Er_{0.05}O_4$ nanoparticles

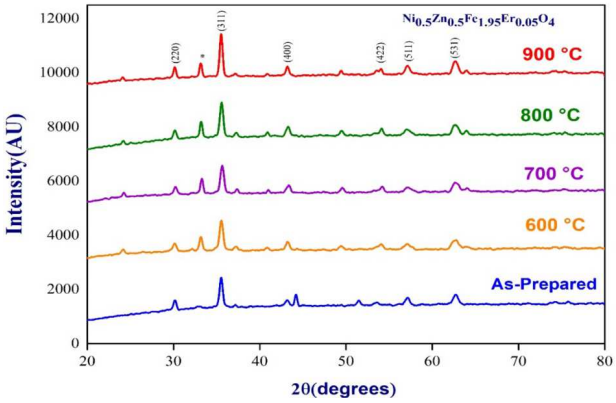

Fig. 2. X-ray patterns of as-prepared and calcinated $Ni_{0.5}Zn_{0.5}Fe_{1.95}Er_{0.05}O_4$ ferrite nanoparticles at 600, 700, 800, & 900 °C

3. Results and Discussions

3.1. XRD analysis

The XRD for the as-prepared and calcinated at four different temperatures of $Ni_{0.5}Zn_{0.5}Fe_{1.95}Er_{0.05}O_4$ spinal nanoparticles have been recorded by Shimadzu XRD-7000, and the XRD plots showed the spinel cubic crystal structure shown in Fig. 2 [26]. The crystallite size for all the prominent peaks using the Scher-

Table 1. **(hkl), 2θ, FWHM, crystallite size, Interplanar spacing of $Ni_{0.5}Zn_{0.5}Fe_{1.95}Er_{0.05}O_4$ nanoparticles of as-prepared and calcinated at 600, 700, 800, & 900 °C**

Calcination temp. (°C)	Miller indices ($h\,k\,l$)	2θ (degrees)	FWHM (radians)	Crystallite size (D) (nm)	Interplanar spacing (d) (Å)
As-prepared	220	30.1651	0.477	17.25189	2.960296
	311	35.5294	0.4509	18.50403	2.525321
	400	43.1822	0.5224	16.35746	2.093421
	–	44.199	0.3195	26.84061	2.048329
	331	51.4854	0.4432	19.90274	1.773708
	422	53.536	0.5622	15.82901	1.710811
	511	57.125	0.5901	15.33019	1.611241
	440	62.7225	0.6869	13.54587	1.480169
600	220	30.1412	0.4037	20.38317	2.962589
	–	33.1768	0.3086	26.86554	2.698127
	311	35.5511	0.4378	19.05887	2.523183
	222	36.5638	0.5976	14.00267	2.455589
	–	41.4817	0.4464	19.0327	2.175118
	400	43.2443	0.4324	19.76635	2.090457
	331	49.4551	0.5238	16.70021	1.841484
	422	53.9934	0.69	12.92332	1.696923
	333	57.1026	0.4857	18.6234	1.61169
	440	62.6621	0.4814	19.32213	1.481397
	531	63.9632	0.4521	20.71885	1.454365
700	220	30.2335	0.4299	19.14509	2.953754
	–	33.2878	0.2724	30.44457	2.689383
	311	35.6465	0.4309	19.36923	2.516649
	222	37.368	0.3481	24.0955	2.404569
	–	40.9908	0.22302	38.03479	2.200026
	400	43.347	0.4908	17.42055	2.085742
	331	49.5793	0.4393	19.92247	1.837162
	422	54.1897	0.39	22.88433	1.691239
	333	57.2215	0.7721	11.72192	1.608624
	440	62.7574	0.7441	12.50691	1.479377
	531	64.0584	0.2284	41.03265	1.452433
800	220	30.17	0.4297	19.15114	2.959827
	–	33.2121	0.2344	35.37315	2.69534
	311	35.5748	0.4569	18.26335	2.521557
	222	37.275	0.3326	25.2115	2.410354
	–	40.9059	0.2611	32.47864	2.204396
	400	43.2821	0.426	20.06593	2.088719
	331	49.5005	0.4133	21.16904	1.839902
	422	54.1242	0.3553	25.11197	1.693131
	333	57.1441	0.4147	21.81617	1.610618
	440	62.7	0.4226	22.01502	1.480593
	531	63.9719	0.331	28.30042	1.454188
900	220	30.1479	0.3751	21.93766	2.961946
	–	33.1609	0.2165	38.29266	2.699384
	311	35.53	0.326	25.5935	2.524633
	222	37.202	0.1428	58.70831	2.414916
	400	43.2123	0.3517	24.29918	2.091931
	331	49.4405	0.2389	36.61388	1.841994
	422	54.0521	0.3311	26.93874	1.695219
	333	57.1464	0.4748	19.0549	1.610559
	440	62.6994	0.4815	19.32195	1.480606
	531	63.9578	0.3379	27.72039	1.454475

Table 2. **Average crystallite size, lattice parameter, unit cell volume, dislocation density and micro strain of $Ni_{0.5}Zn_{0.5}Fe_{1.95}Er_{0.05}O_4$ nanoparticles of as-prepared and calcinated at 600, 700, 800, & 900 °C**

Calcination temp. (°C)	Average crystallite size (D) (nm)	Lattice parameter (a) (Å)	Unit cell volume (V) (Å^3)	Average interplanar spacing (d) (Å)	Dislocation density (δ) $\times 10^{-3}$ nm^{-2}	Micro Strain (ε) $\times 10^{-3}$
As-prepared	17.94522	8.3784	588.1434	2.0254	3.1053	6.1408
600	18.85429	8.3802	588.5227	2.0900	2.8131	4.5201
700	23.32527	8.3852	589.5725	2.0835	1.8380	3.9758
800	24.45058	8.3881	590.1700	2.0871	1.6727	3.4295
900	29.84812	8.3885	590.2703	2.0775	1.1224	3.1728

rer formula, as shown in Eq. (1), was calculated and along with the D, (hkl), 2θ, FWHM, and d values are tabulated in the Table 1 [27]

$$D = \frac{0.89\lambda}{\beta \cos\theta}, \tag{1}$$

where, D is crystallite size, β is full width at half maximum (FWHM), λ is the wavelength equal to 1.54 Å, and θ is the angle of diffraction. It is observed that the crystallite size was increased with the calcination temperature. The average crystallite size for the as-prepared sample was found to be 17.9452 nm (minimum), and the crystallite size for the sample calcinated at 900 °C was equal to 29.8481 nm (maximum).

The parameters such as the micro strain, dislocation density, and lattice parameter of all the samples are tabulated in Table 2. As the ionic radius of an erbium ion higher than a ferric ion, the doping by erbium ions in spinal ferrites increases the micro strain (ε) in nickel-zinc ferrite nanoparticles [28], and the micro strain value was calculated from the equation

$$\varepsilon = \beta/4 \tan\theta. \tag{2}$$

The lattice parameter values were calculated using Eq. (3) [29], and it was found in the interval from 8.3784 to 8.3885 Å

$$a = d(h2 + k2 + l2)^{1/2}. \tag{3}$$

The density of dislocations (δ_D) is calculated from the equation [30]

$$\delta_D = 1/D^2. \tag{4}$$

Metal-oxygen bond lengths and cationic ionic radii at A and B sites were calculated and tabulated in Table 3. The obtained results show that the calcination temperature influences the structural properties, which is in the same line as that in the work by K. Vijaya Kumar *et al.* [31].

Table 3. **Bond lengths and ionic radii in $Ni_{0.5}Zn_{0.5}Fe_{1.95}Er_{0.05}O_4$ nanoparticles of as-prepared and calcinated at 600, 700, 800, & 900 °C**

Calcination temp. (°C)	Bond length of A site-O (Å)	Bond length of B site-O (Å)	Ionic radius (r_A) (Å)	Ionic radius (r_B) (Å)
As-prepared	1.9224	2.0318	0.4228	0.5318
600	1.9236	2.0321	0.4236	0.5321
700	1.9243	2.0334	0.4243	0.5334
800	1.9250	2.0341	0.4250	0.5341
900	1.9251	2.0342	0.4251	0.5342

3.2. SEM analysis

The SEM micrographs of spinel nanoparticles were made by using a feld scanning electron microscope (SEM). The obtained SEM images of all the samples are shown in Fig. 3. We note that the morphology of the grains are not uniform, and flakes with tiny pores are observed [31–32]. The grain size value was found minimum for the sample calcinated at 600 °C to be 46.96 nm. The grain size value was found maximum for the sample calcinated at 900 °C, and it was equal to 177.73 nm (see Table 4). As a result of the substitution of large-size rare-earth metal cations Er^{3+}, we get $Ni_{0.5}Zn_{0.5}Fe_{1.95}Er_{0.05}O_4$ with a significant strain. In this case, the surface area changes, and a reduction in the crystallite and grain sizes occurrs. The average grain size increases with the calcination temperature due to the improved atomic diffusion [33]. It

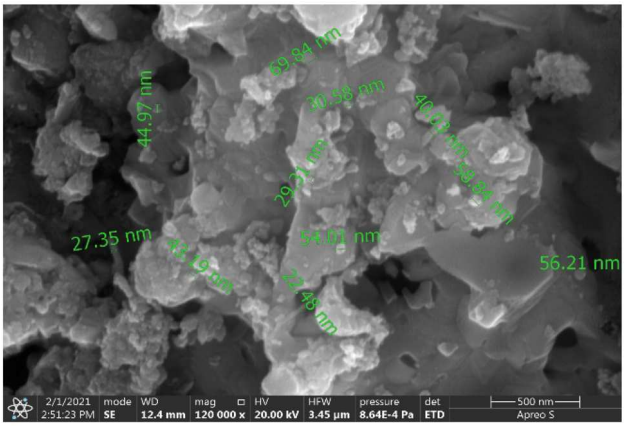

a

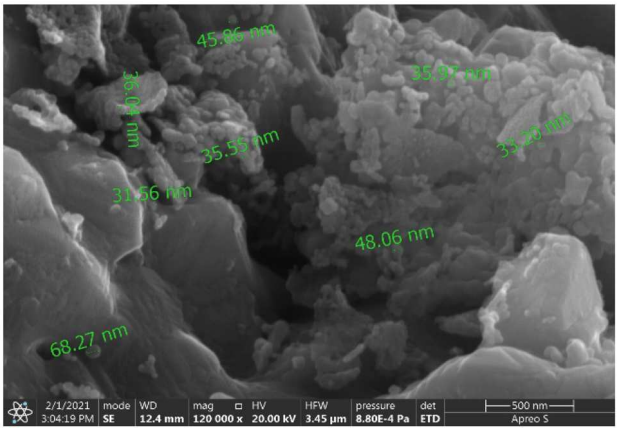

b

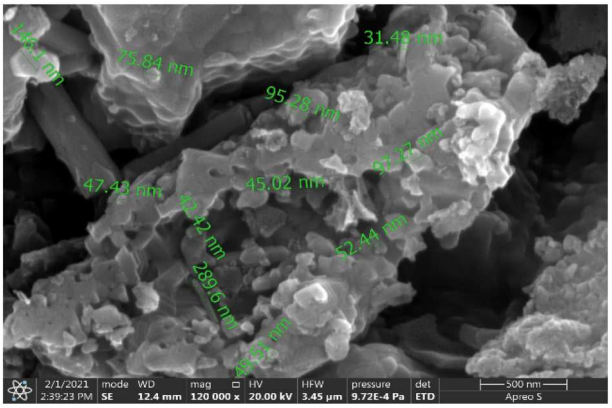

c

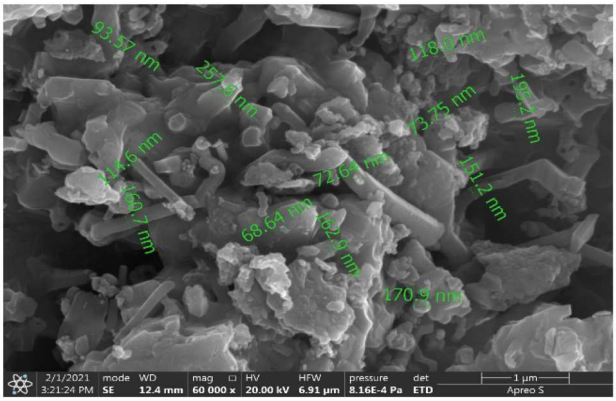

d

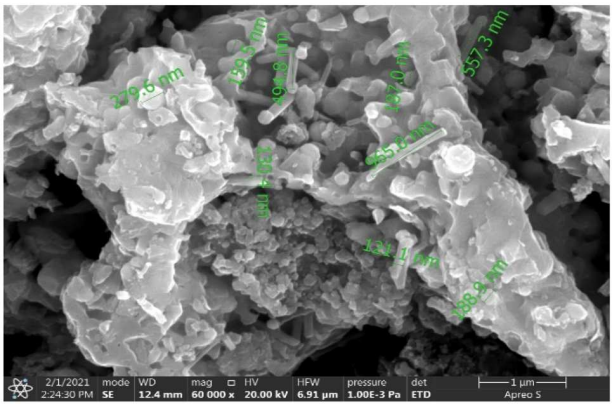

e

Fig. 3. SEM images of $Ni_{0.50.5}Fe_{1.95}Er_{0.05}O_4$ nanoparticles of as-prepared and calcinated at 600, 700, 800, & 900 °C

can be clearly observed from the SEM micro graphs of the as-prepared sample and the sample calcinated at 600 °C that the agglomeration is random with pores and voids, as the crystallization was not yet occurred. Whereas, in the case of SEM micro graphs of the samples calcinated at 700 and 800 °C, the agglomeration was a bit ordered with pores and voids, as the crystallization was as performed. The existence

of agglomeration would be due to the magnetic interaction among the particles [34]. Hence, it may be concluded that the magnetic interaction among the metal ions might be random in the case of the as-prepared sample and the sample calcinated at 600 °C, as the metal ions oriented in a random manner. Whereas in the case of samples calcinated at 700 and 800 °C, the magnetic interaction among the metal ions might be ordered. Further, it was noticed that the formation of nanotubes was initiated in the sample calcinated at 700 °C, and the nanotubes were clearly formed in the micro graph of the sample calcinated at 800 °C. The size of the formed nanotubes appeared very much lower than the size of grains. This observation has created the interest in further studies of this composition at higher calcination temperatures. A similar result was observed in the case of copper-nickel ferrite nanoparticles investigated by Tariq J. Al-Musawi *et. al.* [35].

3.3. FTIR spectroscopy

The FTIR analysis was performed for the identification of a composition of spinal ferrites. The spectra of the as-prepared sample and samples calcinated at different temperatures are presented in Fig. 4. Band peaks in the interval 400–4500 cm^{-1} are shown in the FTIR spectra. The two characteristic absorption bands near 550–600 cm^{-1} and 350–450 cm^{-1} represent the spinel structures of ferrite materials [36].

The peak ν_1 near 550–600 cm^{-1} occurs because of M–O stretching vibrations at A sites, and the peak ν_2 in the interval 350–450 cm^{-1} occurs because of stretching M–O bond vibrations at B sites, that is, not observed in the presented spectra. The found differences in the peak ν_1 can be caused by changes in the M–O bond length, changes at A and B sites, and the transfer of cations among A and B sites [37]. The band around 1600 cm^{-1} can be due to the stretching of N–H bonds. Another peak is available at 3400–3500 cm^{-1} due to the hydroxyl group (OH).

3.4. UV-visible spectroscopy

The UV-Visible spectral analysis for the as-prepared sample and those calcinated at four different temperatures for $Ni_{0.5}Zn_{0.5}Fe_{1.95}Er_{0.05}O_4$ spinal nanoparticles was performed using a Systronics Double Beam UV-Visible Spectrometer. The characteristic absorption peaks of the samples were observed in line with

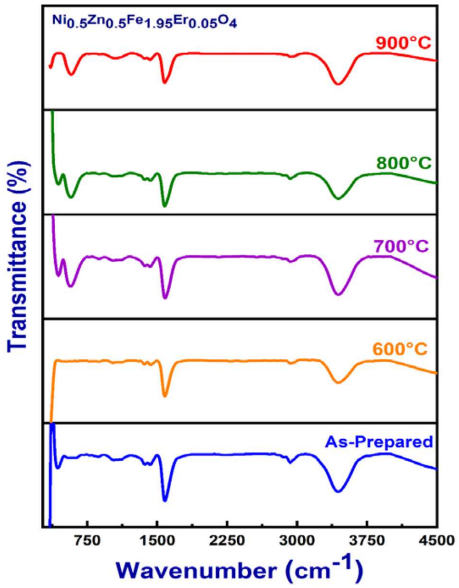

Fig. 4. FTIR spectra of as-prepared and calcinated $Ni_{0.5}Zn_{0.5}Fe_{1.95}Er_{0.05}O_4$ ferrite nanoparticles at 600, 700, 800, & 900 °C

Table 4. **Average grain size and crystallite size of $Ni_{0.5}Zn_{0.5}Fe_{1.95}Er_{0.05}O_4$ nanoparticles of as-prepared and calcinated at 600, 700, 800, & 900 °C**

Calcination temp. (°C)	Average grain size (nm)	Average crystallite size (D) (nm)
As-prepared	46.96	17.94522
600	55.382	18.85429
700	103.623	23.32527
800	159.85	24.45058
900	177.73	29.84812

other spinel ferrites [38]. The energy band gap of the samples (E_g) of all samples was studied by using the Kubelka–Munk theory and were measured using Tauc's relation. The obtained Tauc plots [39] are shown in Fig. 5. We have

$$(\alpha h\nu)^n = A(h\nu - E_g), \tag{5}$$

where α is the absorption coefficient; A is a proportional constant; E_g is the optical band gap of the material, and the exponent n is related to the nature of electronic transitions: $n = 3$ for indirect forbidden transitions; $n = 2$ for indirect allowed transitions; $n = 3/2$ for direct forbidden transitions; $n = 1/2$

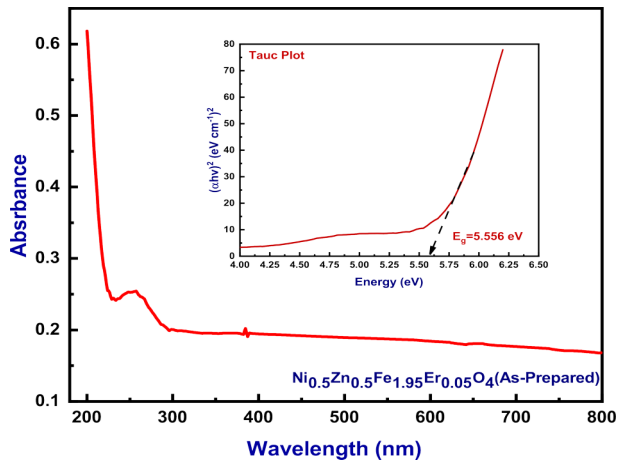

a

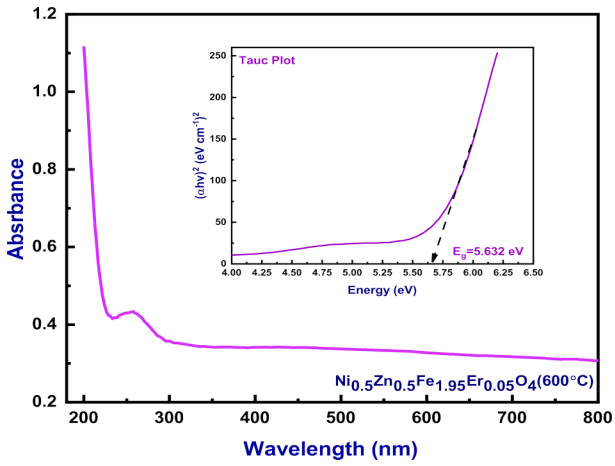

b

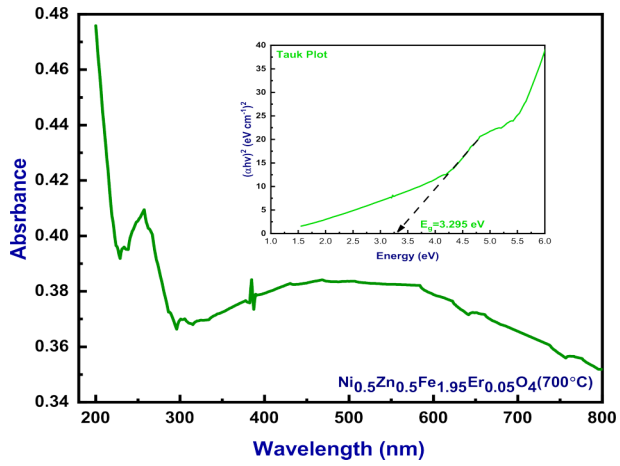

c

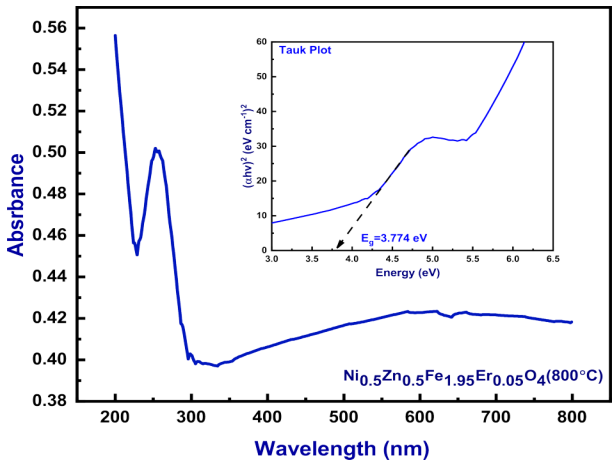

d

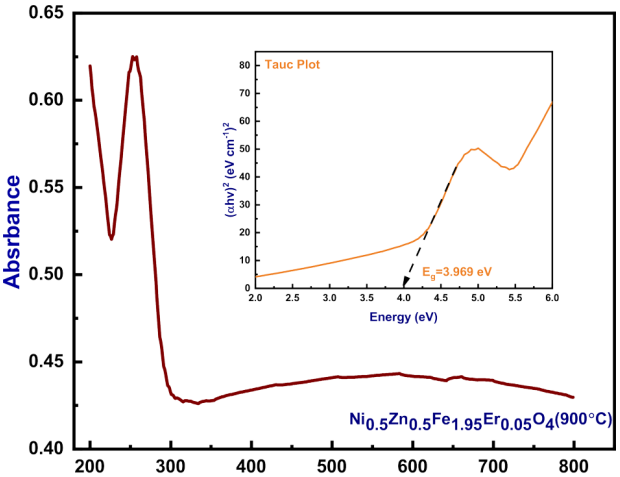

e

Fig. 5. Tauc plots for the as-prepared sample and the samples of $Ni_{0.5}Zn_{0.5}Fe_{1.95}Er_{0.05}O_4$ calcinated at 600, 700, 800, & 900 °C

for direct allowed transitions [39]. The energy band gap (E_g) values for the samples were calculated and tabulated in Table 5. The energy band gap for the as-prepared sample is 5.632 eV, whereas it for the sample calcinated at 900 °C is 3.969 eV. We note that unable energy band gaps in magnetic spinal ferrites are suitable for effective solar photocatalytic reactions [40].

The absorption and transmittance of the samples are shown in Fig. 6. The absorbance can be obtained from the experiment, and the transmittance (I/I_0) can be evaluated from the equation

$$\text{Transmittance (Ts)} = 10^{-A} \times 100. \tag{6}$$

By using the Beer–Lambert's law, the absorption coefficient and extinction coefficient of nanoparticles were calculated from the equations [41–43]

$$I = I_0\, e^{\infty t}, \tag{7}$$

$$A = \log \log \frac{I_0}{I}, \tag{8}$$

$$\alpha = \frac{2.303A}{t}, \tag{9}$$

$$k = \frac{\alpha\lambda}{4\pi}, \tag{10}$$

where I_0 is the incident intensity; I is the transmitted intensity; α is the absorption coefficient; A is the absorbance, and t is the thickness of the sample (1 cm); k is the extinction coefficient, respectively.

The difference in the extinction coefficients of the as-prepared sample and the samples calcinated at different temperatures for $Ni_{0.5}Zn_{0.5}Er_{0.05}Fe_{1.95}O_4$ ferrite are shown in Fig. 7 [44].

The variation of the refractive index of $Ni_{0.5}Zn_{0.5}Er_{0.05}Fe_{1.95}O_4$ ferrite samples with wavelengths in 200–800 nm (UV-visible region) are shown in Fig. 8. We note that the refractive index of all samples increases with the calcination temperature and becomes maximum at the wavelength near 240 nm. The refractive index was measured using the equation [44]

$$n = \frac{1}{T_s} + \sqrt{\frac{1}{T_s - 1}}, \tag{11}$$

Table 5. **Band gap values of $Ni_{0.5}Zn_{0.5}Fe_{1.95}Er_{0.05}O_4$ nanoparticles of as-prepared and calcinated at 600, 700, 800 & 900 °C**

Calcination temperature (°C)	Band gap (E_g) (eV)
As-prepared	5.556
600	5.632
700	3.295
800	3.774
900	3.969

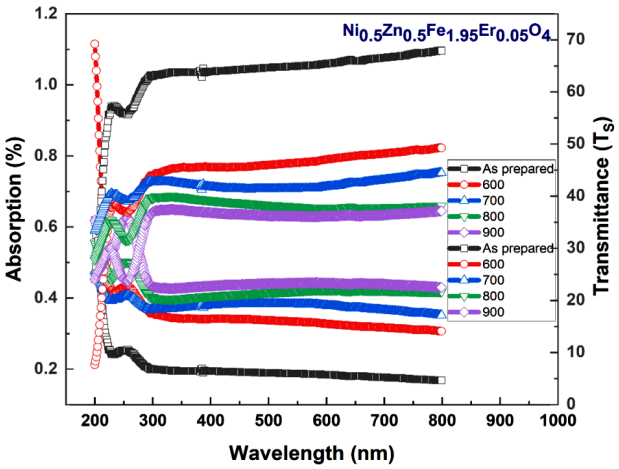

Fig. 6. Absorption and transmittance of the as-prepared sample and the samples calcinated at 600, 700, 800, & 900 °C

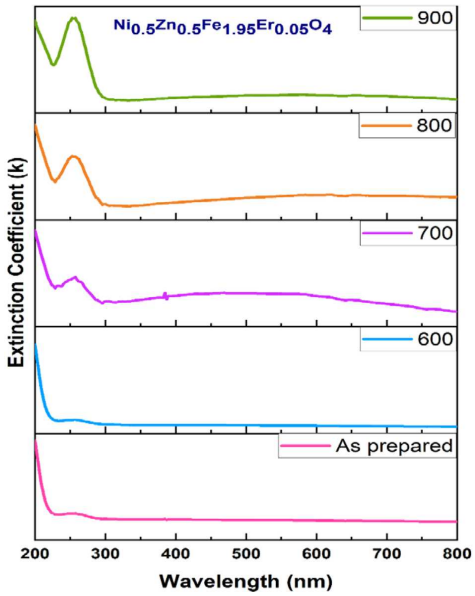

Fig. 7. Absorption and transmittance of the as-prepared sample and the samples calcinated at 600, 700, 800, & 900 °C

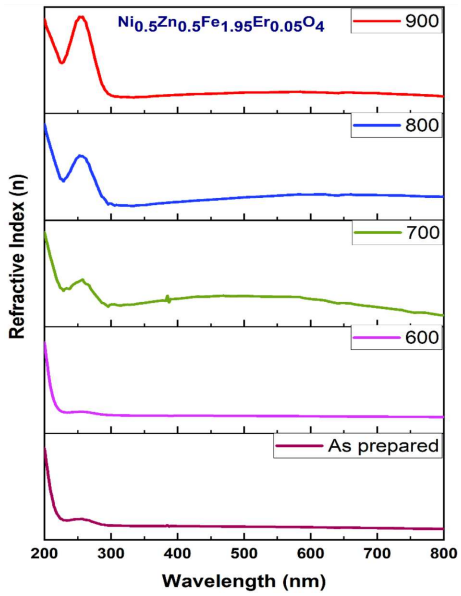

Fig. 8. Refractive Index of the as-prepared sample and the samples calcinated at 600, 700, 800, & 900 °C

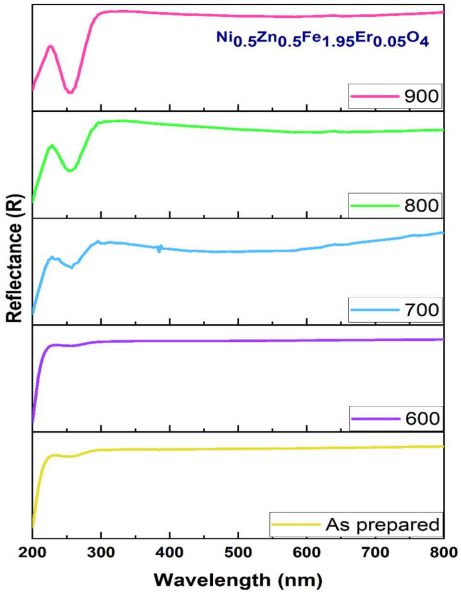

Fig. 9. Reflectance of the as-prepared sample and the samples calcinated at 600, 700, 800, & 900 °C

where n and T_s represent the refractive index and the transmittance.

The variation of the reflectance of $Ni_{0.5}Zn_{0.5}Er_{0.05}Fe_{1.95}O_4$ samples with the wavelength in the interval 200–800 nm in the UV-visible region is shown in Fig. 9. The reflectance of the samples was calculated with the equation [45]

$$R = \frac{(n-1)^2}{(n+1)^2}. \tag{12}$$

It is observed that the reflectance of the samples undergoes the redshift, as the calcination temperature increases [45–46].

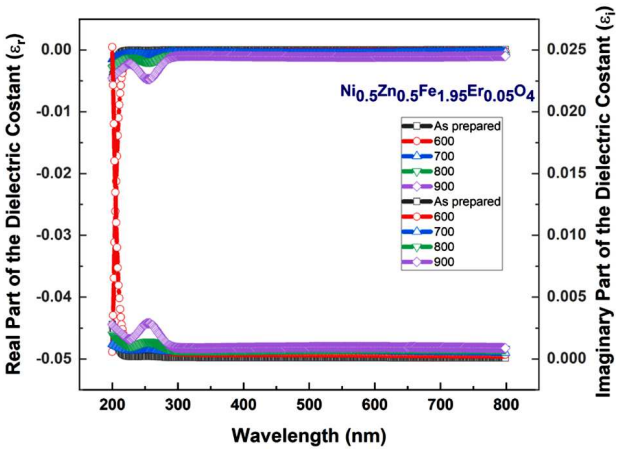

Fig. 10. Real and imaginary parts of dielectric constants of the as-prepared sample and the samples calcinated at 600, 700, 800, & 900 °C

The real and imaginary parts of the dielectric function for the samples are given in Fig. 10 and are seen mainly in the interval 250–330 nm. The curves are fairly flat in the long wavelength region [47]. The real and imaginary parts of the dielectric constant are calculated using the equations

$$\varepsilon_i = 2nk, \tag{13}$$

$$\varepsilon_r = n^2 - k^2, \tag{14}$$

where n and k are the refractive index and the extinction coefficient.

4. Conclusions

1. $Ni_{0.5}Zn_{0.5}Fe_{1.95}Er_{0.05}O_4$ was prepared using the sol-gel autocombustion method and divided into five parts. Four of them were calcinated at four different temperatures.

2. XRD patterns confirm the spinel cubic crystal structure.

3. Average crystallite size is found in the interval from 17.9452 nm to 29.8481 nm from XRD data.

4. Average grain size is determined in the interval 55.382.80–177.73 nm from SEM micro graphs.

5. Nanotubes are formed in the samples calcinated at 700 and 800 °C.

6. The two characteristic absorption bands near 550–600 and 350–450 cm^{-1} in FTIR graphs are seen.

7. The value of energy band gap (E_g) is deternined in the interval 5.556–3.969 5 eV and decreases with the calcinated temperature.

1. D.H.K. Reddy, Y.S. Yun. Spinel ferrite magnetic adsorbents: Alternative future materials for water purification. *Coord. Chem. Rev.* **315**, 90 (2016).
2. S.A.V. Prasad, M. Deepty, P.N. Ramesh, G. Prasad, K. Srinivasarao, C. Srinivas, K. Vijaya Babu, E. Ranjith Kumar, N. Krisha Mohan, D.L. Sastry. Synthesis of MFe_2O_4 (M = Mg^{2+}, Zn^{2+}, Mn^{2+}) spinel ferrites and their structural, elastic and electron magnetic resonance properties. *Ceram. Int.* **44** (9), 10517 (2018).
3. W. Mokhosi, S.Mdlalose, Mngadi, M. Singh, T. Moyo. Assessing the structural, morphological and magnetic properties of polymer-coated magnesium-doped cobalt ferrite ($CoFe_2O_4$) nanoparticles for biomedical application. *J. Phys. Conf. Ser.* **1310**, 012014 (2019).
4. S. Chakrabarty, M. Pal, A. Dutta. Yttrium doped cobalt ferrite nanoparticles: Study of dielectric relaxation and charge carrier dynamics. *Ceram. Int.* **44** (12), 14652 (2018).
5. G. Asab, E.A. Zereffa, T. Abdo Seghne. Synthesis of silica-coated Fe_3O_4 nanoparticles by microemulsion method: Characterization and evaluation of antimicrobial activity. *Int. J. Biomater.* **2020**, 4783612 (2020).
6. M. Anand. Hysteresis in a linear chain of magnetic nanoparticles. *J. Appl. Phys.* **128** (2), 023903 (2020).
7. N. Guijarro, P.Bornoz, M. Prévot, X. Yu, X. Zhu, M. Johnson, K. Sivula. Evaluating spinel ferrites MFe_2O_4 (M = = Cu, Mg, Zn) as photoanodes for solar water oxidation: Prospects and limitations. *Sustain. Energy Fuels* **2** (1), 103 (2018).
8. U. Wongpratat, T. Pannawit, K. Jessada, S. Ekaphan, M. Santi. Effects of nickel and magnesium on electrochemical performances of partial substitution in spinel ferrite. *J. Alloys and Compd.* **831**, 154718 (2020).
9. K.K. Kefeni, T.A. Msagati, T.T. Nkambule, B.B. Mamba. Spinel ferrite nanoparticles and nanocomposites for biomedical applications and their toxicity. *Mater. Sci. Eng. C* **107**, 110314 (2020).
10. I. Rajendran, I. Prakash, M. Venkateswarlu, N. Satyanarayana. Lanthanum ion (La^{3+}) substituted $CoFe_2O_4$ anode material for lithium ion battery applications. *New. J. Chem.* **39** (6), 4601 (2015).
11. M.S.S. Adam, A.M. Hafez, M.M. Khalaf. Rare earth Ce- and Nd-doped spinel nickel ferrites as effective heterogeneous catalysts in the (ep) oxidation of alkenes. *J. Iran. Chem. Soc.* **17** (12), 3237 (2020).
12. K.K. Kefeni, B.B. Mamba. Photocatalytic application of spinel ferrite nanoparticles and nanocomposites in wastewater treatment. *Sustain. Mater. Technol.* **23**, e00140 (2020).
13. S.S. Laha, D. Nanasaheb, T. Gurwinder Singh, C.I. Sathish, J. Yi, A. Dixit. Rare-earth doped iron xide nanostructures for cancer theranostics: Magnetic hyperthermia and magnetic resonance imaging. *Small.* **18** (11), 2104855 (2022).
14. J. Dhumal, M. Phadatare, S.G. Deshmukh, G.S. Shahane. Enhanced heating ability of Fe–Mn–Gd ferrite nanoparticles for magnetic fluid hyperthermia. *J. Mater. Sci. Mater. Electron.* **31** (14), 11457 (2020).
15. B.K. Prashant, B.S. Sandeep, P.K. Pankaj, K.M. Jadhav. induction heating analysis of surface-functionalized nanoscale $CoFe_2O_4$ for magnetic fluid hyperthermia toward noninvasive cancer treatment. *ACS Omega* **5** (36), 23378 (2020).
16. M. Irfan Hussain, M. Xia, K. Akhtar, S.K. Sharma. Ferrite nanoparticles for biomedical applications. *Magnetic Nanoheterostructures. Nanomedicine and Nanotoxicology Springer, Cham.* **693**, 243 (2020).
17. A.K. Nikumbh, R.A. Pawar, D.V. Nighot, G.S. Gugale, M.D. Sangale, M.B. Khanvilkar, A.V. Nagawade. Structural, electrical, magnetic and dielectric properties of rare-earth substituted cobalt ferrites nanoparticles synthesized by the co-precipitation method. *J. Magn. Magn. Mater.* **35**, 201 (2014).
18. G.L. Sun, J.B. Li, J.J. Sun, X.Z. Yang. The influences of Zn^{2+} and some rare-earth ions on the magnetic properties of nickel–zinc ferrites. *J. Magn. Magn. Mater.* **281** (2–3), 173 (2004).
19. N. Rezlescu, E. Rezlescu, C. Pasnicu, M.L. Craus. Effects of the rare-earth ions on some properties of a nickel-zinc ferrite. *J. Phys. Condens. Matter.* **6**, 5707 (1994).
20. J. Jiang, L.C. Li, F. Xu, Y.L. Xie, preparation and magnetic properties of Zn–Cu–Cr–Sm ferrite via a rheological phase reaction method. *Mater. Sci. Eng. B* **137**, 166 (2007).
21. J. Jiang, L.C. Li, F. Xu. Structural analysis and magnetic properties of Gd-doped Li–Ni ferrites prepared using rheological phase reaction method. *J. Rare Earths* **25**, 79 (2007).
22. C. Kumari, D. Hemant Kumar, Farhana Naaz, L. Preeti. Structural and optical properties of nanosized Co substituted Ni ferrites by coprecipitation method. *Phase Transitions* **93** (2), 207 (2020).
23. S. Ravindra, J. Pranat, P. Ravi, S. Srnjay, R.S. Rana, G. Nitish. Synthesis and characterization of nickel ferrite ($NiFe_2O_4$) nanoparticles prepared by sol-gel method. *Mater. Today: Proc.* **2** (4–5), 3750 (2015).
24. A. Sangeetha, K. Vijaya Kumar, G. Nanda Kumar. Effect of annealing temperature on the structural and magnetic properties of $NiFe_2O_4$ nanoferrites. *Adv. Mater. Phys. Chem.* **7**, 19 (2017).
25. A. Hakeem, T. Alshahrani, G. Muhammad, M.H. Alhossainy, A. Laref, R.Y. Khosa, Magnetic, dielectric and struc-

tural properties of spinel ferrites synthesized by sol-gel method. *J. Mater. Res. Technol.* **11**, 158 (2021).
26. K. Vijaya Kumar, A. Chandra, Shekhar Reddy, D. Ravinder. High-frequency dielectric behaviour of erbium substituted Ni–Zn ferrites. *J. Magn. Magn. Mater.* **263**, 121 (2003).
27. Y.B. Kannan, R. Saravanan, N. Srinivasan, I. Ismail. Sintering effect on structural, magnetic and optical properties of $Ni_{0.5}Zn_{0.5}Fe_2O_4$ ferrite nano particles. *J. Magn. Magn. Mater.* **423**, 217 (2017).
28. K. Vijaya Kumar, S.D. Bhavani. Impact of calcination temperature on structural and optical properties of erbium-doped zinc ferrite nanoparticles. *Ph. Transitions.* **95**, 770 (2022).
29. S. Joshi, M. Kumar, S. Chhoker, A. Kumar, M. Singh. Effect of Gd3+ substitution on structural, magnetic, dielectric and optical properties of nanocrystalline $CoFe_2O_4$. *J. Magn. Magn. Mater.* **426**, 252 (2017).
30. K. Vijaya Kumar, S.D. Bhavani, M.A. Shukur. The study of temperature dependent structural and elastic properties of Ni–Zn ferrite nanoparticles. *Bulgarian J. Phys.* **49**, 179 (2022).
31. K. Vijaya Kumar, Sara Durga Bhavani. Influence of calcination temperature on physical and optical properties of nickel chromite nanoparticles. *Science of Sintering* **54**, 457 (2022).
32. S. Fouzar, T. Eftimov, I. Kostova, A. Benmounah, A. Lakhssassi. Effects of temperature on the time responses of strontium aluminates. *Opt. Mater.* **122**, 111619 (2021).
33. M. Atif, S.K. Hasanain, M. Nadeem. Magnetization of sol–gel prepared zinc ferrite nanoparticles: Effects of inversion and particle size. *Solid State Commun.* **138**, 416 (2006).
34. G. Li, X. Zhu, W. Song, Z. Yang, J. Dai, Y. Sun, Y. Fu. Annealing effects on semitransparent and ferromagnetic $ZnFe_2O_4$ nanostructured films by sol–gel. *J. Am. Ceram. Soc.* **94**, 2872 (2011).
35. J. Tariq, Al-Musawi, M. Nezamaddin, T. Mahmoud, S. Zaccheus, B. Davoud. Capability of copper–nickel ferrite nanoparticles loaded onto multiwalled carbon nanotubes to degrade acid blue 113 dye in the sonophotocatalytic treatment process. *Env. Sci. Poll. Res.* **29**, 51703 (2022).
36. A. Gadkari, A. Shinde, T. Vasambekar. Influence of rare-earth ions on structural and magnetic properties of $CdFe_2O_4$ ferrites. *Rare Metals* **29**, 168 (2010).
37. B.M.A. Ahmed, S.T. Bishay, S.I. El-dek, G. Omar. Effect of Ni substitution on the structural and transport properties of $Ni_xMn_{0.8-x}Mg_{0.2}Fe_2O_4$; $0.0 \leq x \leq 0.40$ ferrite. *J. Alloys Compd.* **509**, 805 (2011).
38. M.E. Gouda, W.A.A. Bayoumy. Structural, optical and magnetic properties of Ni aluminates with Co substitution. *Int. J. Sci. Eng. Res.* **6**, 328 (2015).
39. Y. Slimani, H. Güngüneş, M. Nawaz, A. Manikandan, H.S. El Sayed, M.A. Almessiere, H. Sözeri, S.E. Shirsath, I. Ercan, A. Baykal. Magneto-optical and microstructural properties of spinel cubic copper ferrites with Li–Al co substitution. *Ceram. Int.* **44**, 14242 (2018).
40. D.K. Dinkar, B. Das, R. Gopalan, B.S. Dehiya. Magnetic and optical properties of green synthesized nickel ferrite nanoparticles and its applications into photocatalysis. *Nanotech.* **32**, 505725 (2021).
41. H.M. Pathan, J.D. Desai, C.D. Lokhande. Modified chemical deposition and physico-chemical properties of copper sulphide (Cu_2S) thin films. *Appl. Surf. Sci.* **202**, 47 (2002).
42. M. Srivastava, A.K. Ojha, S.Chaubey, A. Materny. Synthesis and optical characterization of nanocrystalline $NiFe_2O_4$ structures. *J. Alloys Compd.* **48**, 515 (2009).
43. S.W. Xue, X.T. Zu, W.L. Zhou, H.X. Deng, X. Xiang, L. Hang, H. Deng. Effects of post-thermal annealing on the optical constants of ZnO thin films. *J. Alloys Compd.* **448**, 21 (2008).
44. K.V. Kumar. Tunable optical bandgap of gadolinium substituted nickel-zinc ferrite nanoparticles-effect of calcination temperature on its optical parameters. *Adv. Mater. Phy. Chem.* **12**, 33 (2022).
45. A. Ashour, N. El-Kadry, S.A. Mahmoud. On the electrical and optical properties of cds films thermally deposited by a modified source. *Thin Solid Films* **269**, 117 (1995).
46. M. Chroma, J. Pinkas, I. Pakutinskiene, A. Beganskiene, A. Kareiva. Processing and characterization of sol–gel fabricated mixed metal aluminates. *Ceram. Int.* **31**, 1123 (2005).
47. P. Marzive, N. Marzieh, D. Zahra, M. Rasoul, G.H.H. Khorrami. Optical and dielectrical properties of nickel ferrite nanoparticles under different synthesized temperature. *Results Phys.* **7**, 3619 (2017).

Received 23.07.23

К. Віджая Кумар, С.Д. Бхавані

ВПЛИВ ТЕМПЕРАТУРИ КАЛЬЦИНУВАННЯ І ДОМІШКИ ЕРБІЮ НА СТРУКТУРНІ ТА ОПТИЧНІ ВЛАСТИВОСТІ НАНОЧАСТИНОК ФЕРИТУ, ЩО МІСТИТЬ НІКЕЛЬ ТА ЦИНК

Синтезовано ферит $Ni_{0,5}Zn_{0,5}Fe_{1,95}Er_{0,05}O_4$ з домішкою ербію. Матеріал поділено на 5 частин. Одна розглядається як контрольний зразок (зразок 1), а інші кальциновано при 600 (зразок 2), 700 (зразок 3), 800 (зразок 4) та 900 °C (зразок 5) з метою визначити зміни структурних та оптичних властивостей зразків залежно від температури кальцинування. Методами дифракції X-променів (XRD) та скануючої електронної мікроскопії (SEM) знайдено, що сполука має кубічну структуру спінелі з просторовою групою Fd3m. Розмір кристалітів є мінімальним у зразку 1 (17,9452 нм) і максимальним у зразку 5 (29,8481 нм). Методом SEM виявлено, що розміри зерен знаходяться в інтервалі від 55,38 до 177,73 нм, а зразок 4 містить нанотрубки. Показано, що енергетична щілина для оптичної смуги сполуки змінюється в межах від 5,556 до 3,969 еВ. Ці результати свідчать про зміни структурних та оптичних властивостей сполуки $Ni_{0,5}Zn_{0,5}Fe_{1,95}Er_{0,05}O_4$ зі зміною температури кальцинування.

Ключові слова: ферит, золь-гель, температура кальцинування, структурні та оптичні властивості.